Movie DR1
Movie DR2
Movie DR3
Movie DR4

GSA DATA REPOSITORY 2014067

SUPPLEMENTARY MATERIALS FOR

Incipient sediment motion across the river to debris-flow transition

Jeff P. Prancevic, Michael P. Lamb, Brian M. Fuller
California Institute of Technology, Division of Geological and Planetary Sciences, 1200 E, California Blvd., MC 170-25, Pasadena, CA, 91125

SUPPLEMENTARY NOTES DR1 & DR2
TABLE DR1
FIGURES DR1-DR4
MOVIES DR1-DR4 (SEPARATE FILES)

SUPPLEMENTARY NOTE DR1 – FRICTION ANGLES

The fluvial sediment transport models (Lamb et al., 2008; Wiberg and Smith, 1987) require an input of grain-pocket friction angle (ϕ_g). The friction angles of individual grains were measured by gluing a single layer of the grains to a flat surface, placing individual loose grains on the glued grains and tilting until the test grain dislodged (Miller and Byrne, 1966). We performed two series of measurements: one in which 24 individual grains were placed in 10 numbered pockets each (totaling 240 measurements) and another in which random grains were dropped on the board (56 measurements). The first series of measurements yielded an average friction angle of ϕ_g = 59.3° ± 14.0°, and the second gave ϕ_g = 57.0° ± 12.4°. The value reported in the main text, ϕ_g = 58.8° ± 13.7°, is the average of all experiments.

To apply the Takahashi (1978) bed-failure model the failure plane was assumed to be at one grain diameter depth as advocated by Takahashi (1978). Porosity was measured by comparing material density to bulk density with similar grain packing as in the experimental flume and found to have a value of 0.43. It is not clear how to measure the friction angle of the failure plane (ϕ_f) for the discrete failures we observed in our experiments and we tried a number of different methods. (1) We built a tilting chute with

the same width as our experimental flume (13-cm) but only 1 m long to allow for very steep slopes. Following the setup for the initial motion experiments, we screed a planar, 10 cm-thick bed and then tilted the short flume slowly until a dry granular avalanche occurred. We performed this test ten times and the experiments yielded an avalanche angle of $\phi_f = 45.6° \pm 1.6°$ (100 cm bed length in Fig. DR4). With such a low avalanche angle, the Takahashi model underpredicts stability from our experiments. (2) To test for the effect of water lubrication and buoyancy, we performed the same tests with the 1-m long chute but this time completely submerged in static water. The average friction angle measured was $\phi_f = 45.4º$, within one standard deviation of the dry measurements. (3) To test whether the length of the chute influenced the friction angle, we performed a single experiment in which we placed a dry screed bed in the larger flume used for experiments and raised the upstream end until the bed failed. The resulting avalanche angle was $\phi_f = 44.5º$, within the range reported for the first series of experiments. (4) Finally, to mimic our observed experimental failure conditions in which a single layer initially fails with some discrete length, we modified our short flume accordingly: we glued two layers of gravel at the lower half of the tilt table, and only a single layer of gravel in the upper half of the tilt table. We placed variable amounts of loose gravel extended upstream of the double-thick gravel and performed similar tilting experiments as above. The resulting avalanche angles were $\phi_f = 48.9° \pm 1.2°$ for a 22-cm length, 1-grain diameter deep loose bed, and $\phi_f = 55.1º \pm 3.1°$ for a 10-cm length, 1-grain diameter deep loose bed (Fig. DR4). All cases had a 13-cm chute width. We chose the latter angle for use in the Takahashi model, because these relatively short failure initiations are what we most commonly observed in our experiments (e.g., Movie DR4).

SUPPLEMENTARY NOTE DR2 – MEASURING GRAIN VELOCITY

To measure grain motion at the surface and at depth within the two transport regimes we collected video from cameras oriented orthogonal to the flume's clear sidewall. We made displacement maps by running statistical correlations between successive frames using a 10-pixel (5 mm) correlation window in COSI-Corr software (Leprince et al., 2007). These maps were reduced to vertical velocity profiles by summing the total displacement in the rows and dividing by the number of columns and the elapsed time. Short video clips (Movies DR1 & DR2) provided 122 and 194 independent frames for particle correlations (25 fps) for fluvial transport and bed failure, respectively (Fig. 2).

REFERENCES CITED

Lamb, M.P., Dietrich, W.E., and Venditti, J.G., 2008, Is the critical Shields stress for incipient sediment motion dependent on channel-bed slope?: Journal Of Geophysical Research-Earth Surface, v. 113, no. F2, p. F02008, doi: 10.1029/2007JF000831.

Leprince, S., Barbot, S., Ayoub, F., and Avouac, J., 2007, Automatic and precise orthorectification, coregistration, and subpixel correlation of satellite images, application to ground deformation measurements: Geoscience and Remote Sensing, IEEE Transactions on, v. 45, no. 6, p. 1529–1558.

Miller, R.L., and Byrne, R.J., 1966, The Angle of Repose for a Single Grain on a Fixed Rough Bed: Sedimentology, v. 6, no. 4, p. 303–314, doi: 10.1111/j.1365-3091.1966.tb01897.x.

Takahashi, T., 1978, Mechanical Characteristics of Debris Flow: J Hydr Eng Div-ASCE, v. 104, no. HY8, p. 1153–1169.

Wiberg, P.L., and Smith, J.D., 1987, Calculations of the Critical Shear Stress for Motion of Uniform and Heterogeneous Sediments: Water Resources Research, v. 23, no. 8, p. 1471–1480, doi: 10.1029/WR023i008p01471.

Table DR1. List of experimental conditions and measurements. For cases in which both flow-depth methods were used, the difference between them was less than 30%, error that is smaller than variance between repeat experiments. We found that both flow-depth methods worked well for low slopes, but favored the continuity method because it did not require labor-intensive image analysis. For the steepest slopes ($\theta > 22^{\circ}$) we favored the interface-mapping method for depth as subsurface flow dominated the total discharge resulting in larger error in calculated surface-flow discharge

Bed Angle, θ (º)	Channel width (cm)	Number of experi-ments	Number of sediment flux measure-ments	Depth measurement method	Particle Reynolds Number, Re_p	Mode of transport	Flow depth, H (cm)	Critical Shields stress, τ_c^*
1.8	35	1	7	Continuity	1350	River	2.63	0.034
3.2	35	2	17	Continuity	1612	River	2.11	0.047
5.6	35	5	37	Continuity	1820	River	1.54	0.061
5.9	13	2	12	Both	1856	River	1.52	0.063
6.8	35	1	10	Continuity	2025	River	1.57	0.075
8.0	35	5	17	Continuity	2087	River	1.42	0.080
9.8	35	3	11	Continuity	2243	River	1.34	0.093
11.5	13, 35	3, 1	4, 1	Both	2463	River	1.38	0.113
12.4	35	2	5	Continuity	2413	River	1.23	0.109
13.5	35	2	3	Continuity	2485	River	1.20	0.116
14.2	13	2	3	Both	2569	River	1.22	0.125
15.6	35	1	4	Continuity	2701	River	1.23	0.139
16.9	13	2	5	Both	2715	River	1.15	0.141
19.6	13	2	5	Both	3029	River	1.24	0.178
22.3	13	2	N/A	Interface mapping	3273	Transitional	1.28	0.211
25.2	13	2	N/A	Interface mapping	3426	Bed failure	1.25	0.238
27.9	13	2	N/A	Interface mapping	2909	Bed failure	0.82	0.176
30.1	13	2	N/A	Interface mapping	2618	Bed failure	0.62	0.145
33.0	13	2	N/A	Interface mapping	1550	Bed failure	0.20	0.053

SUPPORTING FIGURES

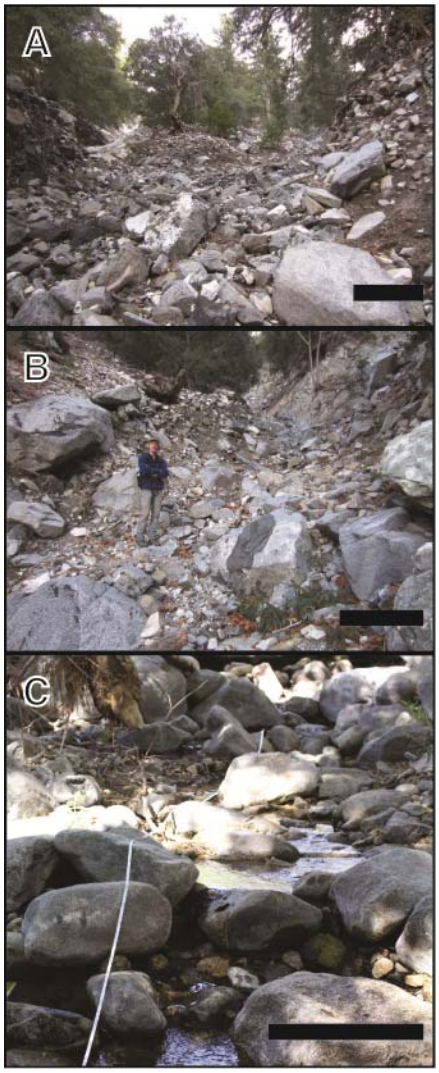

Figure DR1. Photographs from steep channels in the San Gabriel Mountains, CA, USA (A & B: 34º14’50” N, 118º06’03” W; C: 34º15’58” N, 118º08’38” W). Scale bars correspond to approximately one meter in the foreground. A) Channel reach with a bed slope of 31º containing unsorted, angular boulders and cobbles with no apparent development of fluvial bed morphology. B) Channel reach at bed slope of 24º where boulders are more rounded and are sorted into more uniform distributions within the active channel. C) Channel reach at bed slope of 3.2º exhibiting fluvial step-pool bedforms with steps composed of rounded boulders and finer grains present in the pools.

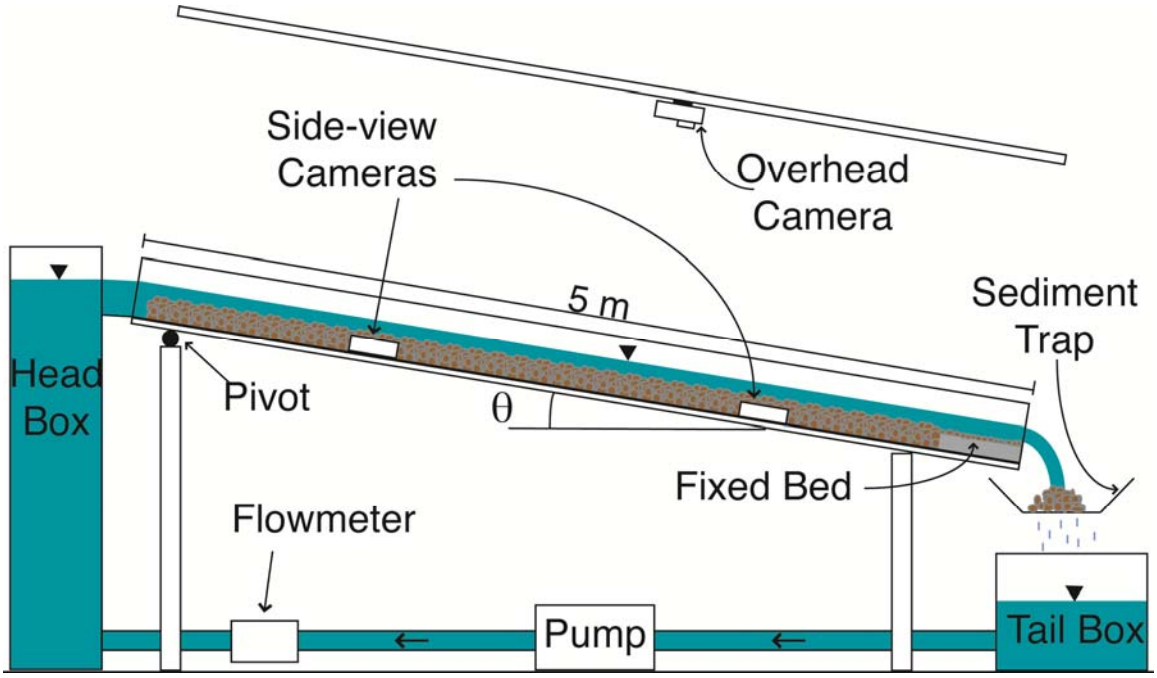

Figure DR2. Flume schematic. Not to scale. In experiments with fluvial transport we used the sediment trap for one to three minutes beginning two minutes after each increase in discharge. Total discharge was measured using a flow meter in the plumbing. The overhead camera was used to track dye pulses in order to measure flow velocity. The photographs used to map sediment-water and water-air interfaces were taken with the side-view cameras.

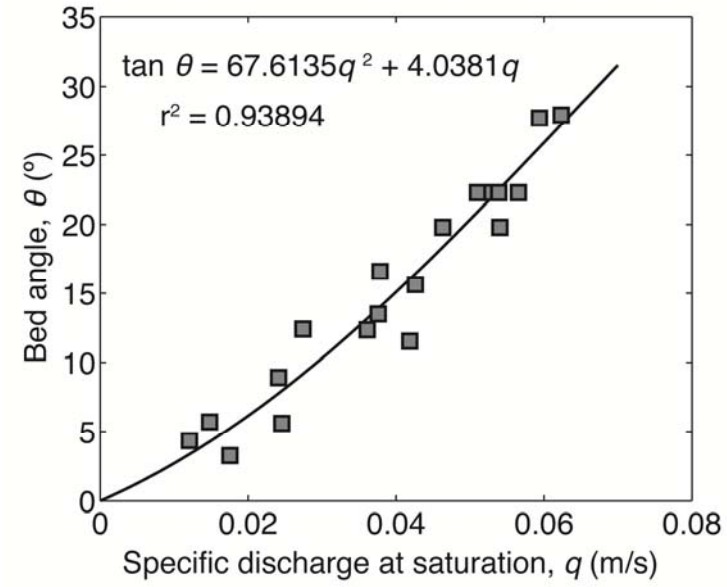

Figure DR3. Bed slope as a function of measured saturated subsurface discharge. Because of the high Reynolds numbers in the experiments (~200 to 750), the linear Darcy relationship for subsurface discharge does not hold. Instead, we use a calibrated Forchheimer equation, shown in the upper left corner, to calculate the subsurface discharge for each slope. This equation is the best-fit second-degree polynomial (solid black line) to the displayed data. Surface-flow discharge was calculated by subtracting the sub-surface discharge using the calibrated Forchheimer equation from the total discharge.

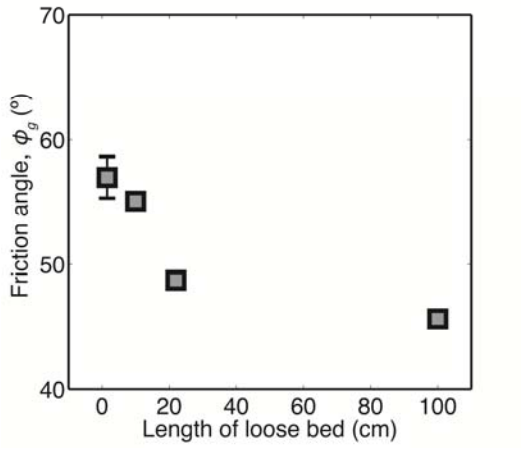

Figure DR4. Bed friction angle as function of the length of the loose bed. Each data point is representative of a series of tilt table experiments in which one or several loose particles were placed on a bed of fixed gravel. For the case with a 1.5 cm length of loose bed, a single particle with D = 1.5 cm was dropped at random on a bed and allowed to settle before tilting the bed. The experiments with longer loose beds were performed by having two layers of glued particles on the tilt table, the second acting as a downstream buttress to the length of loose grains. The error bars represent the standard error of the experiment series, and are hidden behind symbols where errors are small.

SUPPORTING MOVIE CAPTIONS

Example videos of fluvial sediment transport, stabilizing bed failures, and sustained bed failures.

Movie DR1. 39 s video showing fluvial sediment transport at a steep slope (17º bed angle). Shown first at normal playback speed, then at 20% speed.

Movie DR2. 26 s video showing a bed failure near the transitional slope (25º). Failures initiate repeatedly but quickly stabilize. Shown first at normal playback speed, then at 20% speed.

Movie DR3. 37 s video showing a sustained bed failure within the debris flow regime (33º). A single failure is initiated then maintained as the flow runs out the end of the flume. Shown first at normal playback speed, then at 20% speed.

Movie DR4. 43 s video showing an initiation of a bed failure near the transitional slope (25º). At 00:03 (normal playback) and 00:23 (10% speed) a cluster of 5 grains in length destabilizes in the right third of the frame. This destabilization then spreads throughout the rest of frame as the bed fails.